Bol. Soc. Paran. Mat.
©SPM – E-ISSN-2175-1188
SPM: www.spm.uem.br/bspm

(3s.) **v. 2025 (43) 3** : 1–18.
ISSN-0037-8712
doi:10.5269/bspm.78462

Comparison of some a posteriori error estimators

Ilyas Naji

ABSTRACT: The idea of *a posteriori* error estimates based on the reconstruction of the equilibrated potential and/or equilibrated flux goes back to the Prager-Synge equality for the Poisson equation $-\Delta p = f$. This identity is valid for all $v \in H_0^1(\Omega)$ and all $\mathbf{u} \in H(\mathrm{div}, \Omega)$ such that $\mathrm{div}\mathbf{u} + f = 0$, and given by

$$\|\mathbf{u} - \nabla v\|_{0,\Omega}^2 = \|\mathbf{u} - \nabla p\|_{0,\Omega}^2 + \|\nabla p - \nabla v\|_{0,\Omega}^2.$$

It follows that, to obtain such estimate, we need to reconstruct a so-called equilibrated flux; $\mathbf{u} \in H(\mathrm{div}; \Omega)$ satisfying the equilibrium condition $\mathrm{div}\mathbf{u} + f = 0$ and such that $\mathbf{u} - \nabla p$ is as small as possible, and/or reconstruct a potential v in $H_0^1(\Omega)$.
In all cases, to have an estimate, which is said "by reconstruction", it is necessary to have at the end an equilibrated, flux and potential. Now, the question is: is it better to work with a numerical method that allows us to have an equilibrated quantities and in this case there is no need to reconstruct, or else, do we use a method where, we do not have an equilibrated solutions such as the Discontinuous Galerkin method, and in this case it is necessary to reconstruct the two variables? We first compare two types of error estimators: the classical residual-based estimators, which do not require any reconstruction, and the reconstruction-based estimators, in the context of a diffusion problem. Then, using various numerical approximation methods, we proceed to compare the different reconstruction-based estimators.

Key Words: Comparison, a posteriori, error, estimates, residual, reconstruction.

Contents

2010 *Mathematics Subject Classification:* 65N15, 65N30, 65N50, 65N12.
Submitted August 17, 2025. Published October 07, 2025

1. Introduction

A posteriori error estimates were first introduced in 1978 by Babuška and Rheinboldt [4], and since then have become an essential component of adaptive finite element methods. Their development is motivated by the need to control the discretization error while maintaining computational efficiency. Among the numerous families of a posteriori error estimates, the most commonly used approaches are: residual-based estimators [26,27,2,8,10,21,7,17], reconstruction-based estimators [12,23,9,28,15,22,24,25, 6], hierarchical estimators [3,1,19,29], and local problem-based estimators [2,5,18], among others.

In this work, we focus on two of the most prominent approaches: classical residual-based estimators and estimators based on flux and potential reconstructions. For mixed finite element methods, residual-based estimators are typically constructed from residual equations, orthogonality properties, quasi-interpolation operators, and decompositions of vector fields in $H(\mathrm{div})$; see [13,30,17] for detailed treatments. In contrast, reconstruction-based estimators rely on the concept of equilibrated quantities: fluxes and potentials that are reconstructed to satisfy certain compatibility and regularity conditions.

Consider the Poisson problem $-\Delta p = f$ with homogeneous Dirichlet boundary conditions. Let p_h be a numerical approximation of p, and let $\mathbf{u}_h$ be an approximation of the flux $-\nabla p$. A *potential reconstruction* is a function $\bar{p}_h \in H_0^1(\Omega)$, reconstructed from p_h, which aims to minimize the norm $\|u_h + \nabla \bar{p}_h\|$. Similarly, an *equilibrated flux reconstruction* is a function $\bar{u}_h \in H(\mathrm{div};\Omega)$, constructed from u_h, that satisfies $\mathrm{div}\bar{u}_h = f$ (typically in a local or global sense).

For instance, using the lowest-order Raviart-Thomas finite elements RT_0, one obtains a flux in $H(\mathrm{div};\Omega)$ that is already equilibrated (i.e., satisfying the divergence constraint), but the potential is discontinuous and belongs only to a piecewise constant space. Consequently, only the potential needs to be reconstructed. In contrast, if the approximation is obtained using the discontinuous Galerkin (DG) method, neither the flux nor the potential is conforming, and both require reconstruction to satisfy the conditions mentioned above.

This observation naturally raises the following question: when aiming for accurate and reliable error estimates, should we adopt numerical methods that produce equilibrated quantities directly, or instead use nonconforming methods and reconstruct both variables afterward? Before addressing this issue, we begin by comparing residual-based error estimates with reconstruction-based error estimates in the context of elliptic problems.

The objective of this work is the comparison between:

- Firstly, **the classical residual type** estimation for a mixed formulation and **estimation by reconstruction**.
- Secondly, a posteriori error estimates by reconstruction using **different approximations**.

The remainder of this paper is organized as follows. The rest of Section 1 introduces the model problem along with the main notations used throughout the paper. In Section 2, we recall the classical residual-based a posteriori error estimators. Section 3 presents general results related to reconstruction-based error indicators. Section 4 provides a comparative discussion of the two classes of estimators. Section 5 is devoted to finite element approximations and the construction of associated reconstructions, namely Raviart-Thomas elements, Crouzeix-Raviart elements, and the Discontinuous Galerkin method. In Section 6, we present a set of numerical experiments that illustrate and compare the behavior of the estimators under various configurations. Finally, Section 7 provides a concluding summary of the results.

We consider the following model problem

$$\begin{cases} \mathbf{u} + \mathbf{K}\nabla p = 0 \quad in \quad \Omega \\ \mathrm{div}\mathbf{u} = f \quad in \quad \Omega \end{cases} \tag{1.1}$$

where $\Omega \subset \mathbb{R}^2$ is a bounded open polygonal domain, $\mathbf{K}$ is a symmetric, bounded, and uniformly positive definite tensor and $f \in L^2(\Omega)$.

Notation

The Sobolev space $H^1(\Omega)$ consists of functions in $L^2(\Omega)$ whose weak gradients lie in $\left(L^2(\Omega)\right)^2$, and $H_0^1(\Omega)$ represents the subspace of such functions with zero trace on the boundary.
For any subdomain ω of Ω, $(\cdot,\cdot)_\omega$ denotes the $L^2(\omega)$ inner product, with $\|\cdot\|_\omega$ as the corresponding norm (when $\omega = \Omega$, we drop the subscript), and $|\omega|$ is the Lebesgue measure of ω. For $\omega \subset \mathbb{R}$, $\langle\cdot,\cdot\rangle_\omega$ represents either the one-dimensional $L^2(\omega)$ inner product or the appropriate duality pairing on ω.
In this paper, we will use a triangulation $\mathcal{T}_h$, which for all $h > 0$, consists of closed triangles T such that $\overline{\Omega} = \bigcup_{T\in\mathcal{T}_h} T$. We assume that the triangulations $\mathcal{T}_h$ are conforming, i.e., if $K, L \in \mathcal{T}_h$, with $K \neq L$, then $K \cap L$ is either empty, a common edge, or a common vertex of K and L. Let h_K denote the diameter of K, and let $h := \max_{K\in\mathcal{T}_h} h_K$ the mesh size.
We denote by $P_k(\mathcal{T}_h) := \{v \in L^2(\Omega) \mid v|_T \in \mathbb{P}_k(T),\ \forall T \in \mathcal{T}_h\}$, where $\mathbb{P}_k(T)$ denotes the polynomials of total degree $\leq k$ on T. The diffusion tensor K is assumed to be in $P_0(\mathcal{T}_h)$. We also denote by $H^1(\mathcal{T}_h) := \{v \in L^2(\Omega) \mid v|_T \in H^1(T),\ \forall T \in \mathcal{T}_h\}$ the broken Sobolev space of order one on $\mathcal{T}_h$, and by $RT_0(\mathcal{T}_h) := \{\mathbf{v} \in H(\mathrm{div},\Omega) \mid \mathbf{v}|_T \in RT_0(T),\ \forall T \in \mathcal{T}_h\}$, the lowest-order Raviart–Thomas finite element space, with $RT_0(T) = \mathbb{P}_0(T)^2 + \mathbf{x}\,\mathbb{P}_0(T)$. The operator $\Pi_0 : L^2(\Omega) \to P_0(\mathcal{T}_h)$ denotes the L^2-orthogonal projection, i.e. $\int_\Omega (v - \Pi_0 v)\, w\, dx = 0 \quad \forall\, w \in P_0(\mathcal{T}_h)$, which is equivalently characterized by $(\Pi_0 v)|_T = \frac{1}{|T|}\int_T v\, dx \quad \forall T \in \mathcal{T}_h$.
We denote by $\mathcal{E}_h$ the set of all edges of $\mathcal{T}_h$, by $\mathcal{E}_h^{\mathrm{int}}$ the set of interior edges, by $\mathcal{E}_h^{\mathrm{ext}}$ the set of boundary edges, and by $\mathcal{E}_K$ the set of all edges of an element $K \in \mathcal{T}_h$; h_e denotes the diameter of $e \in \mathcal{E}_h$. For $e \in \mathcal{E}_h^{\mathrm{int}}$, there are $T^-$and T^+ in $\mathcal{T}_h$ such that $e = T^- \cap T^+$. Let $\mathbf{n}_e$ be the unit normal vector to e pointing from T^-towards T^+. For a double-valued function v on e, its jump is defined as $[v] = v^- - v^+$with $v^\pm = v|_{T^\pm}$.

A mixed formulation of this problem consists to

$$\left\{\begin{array}{l} find\ \ (\mathbf{u},p) \in H(div;\Omega)\times L^2(\Omega)\ such\ that \\ \displaystyle\int_\Omega \mathbf{K}^{-1}\mathbf{u}\cdot\mathbf{q} - \int_\Omega p\,\mathrm{div}\mathbf{q} = 0, \quad \forall \mathbf{q} \in H(div;\Omega) \\ \displaystyle\int_\Omega v\,\mathrm{div}\mathbf{u} = \int_\Omega f\,v, \quad \forall v \in L^2(\Omega) \end{array}\right. \tag{1.2}$$

The problem (1.2) is well posed thanks to the inf-sup condition cf. [11].

An approximation of the problem (1.2) can be given by the elements of Raviart-Thomas [11]:

$$\left\{\begin{array}{l} find\ \ \mathbf{u}_h \in Q_h\ \ and\ \ p_h \in V_h\ \ solutions\ \ of \\ \displaystyle\int_\Omega \mathbf{K}^{-1}\mathbf{u}_h\mathbf{q}_h dx - \int_\Omega p_h \mathrm{div}\mathbf{q}_h = 0 \quad \forall \mathbf{q}_h \in Q_h \\ \displaystyle\int_\Omega (\mathrm{div}\mathbf{u}_h - f)v_h dx = 0 \quad \forall v_h \in V_h \end{array}\right. \tag{1.3}$$

where, $Q_h := RT_0(\mathcal{T}_h)$, $V_h := P_0(\mathcal{T}_h)$.

We also define the semi-norm on $H^1(\Omega)$ by

$$|||v|||_1 := \|\mathbf{K}^{1/2}\nabla v\|, \qquad \forall v \in H^1(\Omega) \tag{1.4}$$

which becomes a norm thanks to the inequality of Poincaré-Friedrichs. We define the standard energy norm for vectors in $(L^2(\Omega))^2$ by.

$$|||\mathbf{q}|||_\star := \|\mathbf{K}^{-1/2}\mathbf{q}\|, \qquad \forall \mathbf{q} \in (L^2(\Omega))^2. \tag{1.5}$$

The div-energy norm for vectors is defined:

$$|||\mathbf{q}|||^2_{\star,div} := |||\mathbf{q}|||^2_\star + \|div\mathbf{q}\|^2, \qquad \forall \mathbf{q} \in H(\mathrm{div},\Omega). \tag{1.6}$$

2. The residual based error estimator

The development of a posteriori estimates for mixed formulations is generally more challenging than estimates for standard formulations. This is mainly due to the peculiarities of the space $H(\mathrm{div};\Omega)$. More specifically, after integration by parts, the upper bound of the interpolation error in the L^2 norm in terms of the $H(\mathrm{div})$ norm is not optimal. Moreover, the traces of functions in $H(\mathrm{div};\Omega)$ are in $H^{-1/2}(\partial\Omega) \not\subset L^2(\partial\Omega)$ as opposed to the traces of $H^1(\Omega)$ which are in $H^{1/2}(\partial\Omega) \subset L^2(\partial\Omega)$. To overcome these difficulties, the authors in [13,30] considered the Helmholtz decomposition of the space $H(\mathrm{div};\Omega)$. This allowed to have the following error estimation result, where the error indicators can be easily calculated thanks to the available finite element approximation $(\mathbf{u}_h, p_h)$.

Proposition 2.1 *Let $(\mathbf{u}, p)$ solution of the problem (1.2) and $(\mathbf{u}_h, p_h)$ solution of the problem (1.3) then it exists a positif constant C_R independent of h such that:*

$$\|p - p_h\|_0^2 + |||\mathbf{u} - \mathbf{u}_h|||_{\star,div}^2 \leq C_R \left(\widehat{\eta^{Res}}\right)^2$$

where

$$\left(\widehat{\eta^{Res}}\right)^2 := \sum_{T\in\mathcal{T}_h} (\eta_{\mathrm{div},T}^{Res})^2 + (\eta_{D,T}^{Res})^2 + (\eta_{S,T}^{Res})^2 \tag{2.1}$$

$$\eta_{\mathrm{div},T}^{Res} = \|f - \mathrm{div}\mathbf{u}_h\|_{0,T} \tag{2.2}$$

$$\eta_{D,T}^{Res} = h_T \|\mathbf{u}_h\|_{0,T} \tag{2.3}$$

$$\eta_{S,T}^{Res} = h_e^{1/2} \|[K^{-1}\mathbf{u}_h.\mathbf{t}_{e_i}]_J\|_{0,\partial T} \tag{2.4}$$

Remark 2.1

- The indicator $\eta_{Div,T}^{Res}$ represents the residual of the second equation of (1.1). Using the second equation of (1.3), this indicator can also be seen as a data oscillation indicator since $\mathrm{div}\,\mathbf{u}_h = \Pi_0 f$.
- $\eta_{D,T}^{Res}$ represents the residual of the Darcy equation with $\nabla p_h = 0$ since p_h is piecewise constant.
- $\eta_{S,T}^{Res}$ is the jump of the tangential trace of u_h. The normal trace being continuous, since the approximation is conforming in $H(\mathrm{div})$ (which is not the case for the tangential trace).

3. General results for reconstruction-based a posteriori error indicators

In this section, we present the general results concerning error estimates by reconstruction (cf. [28]), in which an upper bound for the error on the flux is provided in the L^2 and $H(\mathrm{div})$ norms, while an upper bound for the potential is also given in the H^1 norm. This result is referred to as general in the sense that it depends neither on the approximation method employed nor on the corresponding reconstruction procedure. We first start by defining what is meant by an equilibrated flux and potential.

Definition 3.1

- Let p_h be the approximation of $p \in H_0^1(\Omega)$ obtained by a numerical method. We will call the potential reconstruction any function s_h constructed from p_h which satisfies

$$s_h \in H_0^1(\Omega).$$

- We will call the equilibrated flux reconstruction any function $\boldsymbol{\sigma}_h$ constructed from $\mathbf{u}_h$ the approximation of the exact flux $\mathbf{u}$, verifying $\sigma_{\mathbf{h}} \in H_f(\mathrm{div},\Omega)$ where

$$H_f(\mathrm{div},\Omega) := \{\sigma_{\mathbf{h}} \in H(\mathrm{div},\Omega) / \int_K \mathrm{div}\sigma_{\mathbf{h}} = \int_K f, \ \ \forall K \in \mathcal{T}_h\} \tag{3.1}$$

Proposition 3.1 *Let* $(\mathbf{u}, p)$ *be the solution of (1.2),* $(\sigma_{\mathbf{h}}, s_h)$ *equilibrated in the sense of definition 3.1. Then*

$$\begin{aligned} |||\mathbf{u} - \sigma_{\mathbf{h}}|||_{\star}^2 &\leq \widehat{\eta^{eq}}_{F,L^2}^2 \\ |||\mathbf{u} - \sigma_{\mathbf{h}}|||_{\star,div}^2 &\leq \widehat{\eta^{eq}}_{F,\mathrm{div}}^2 \\ |||p - s_h|||_1^2 &\leq \widehat{\eta^{eq}}_{P,H^1}^2 \end{aligned} \tag{3.2}$$

where:

$$\widehat{\eta^{eq}}_{F,L^2}^2 := \sum_{T\in\mathcal{T}_h} \left((\eta_{P,T}^{eq})^2 + (\eta_{R,T}^{eq})^2 \right)$$

$$\widehat{\eta^{eq}}_{F,\mathrm{div}}^2 := \sum_{T\in\mathcal{T}_h} \left((\eta_{P,T}^{eq})^2 + (\eta_{R,T}^{eq})^2 + (\eta_{Div,T}^{eq})^2 \right),$$

$$\widehat{\eta^{eq}}_{P,H^1}^2 := \sum_{T\in\mathcal{T}_h} \left(\eta_{P,T}^{eq} + \eta_{R,T}^{eq} \right)^2,$$

the potential estimator is given by:

$$\eta_{P,T}^{eq} := |||\sigma_{\mathbf{h}} + \mathbf{K}\nabla(s_h)|||_{\star,T}, \tag{3.3}$$

the residual estimator (oscillation) by:

$$\eta_{R,T}^{eq} := \frac{h_T}{\pi c_{K,T}^{1/2}} |||f - \operatorname{div}\sigma_{\mathbf{h}}\|_{0,T}, \tag{3.4}$$

and the divergence estimator by:

$$\eta_{Div,T}^{eq} := \|f - \operatorname{div}\sigma_{\mathbf{h}}\|_{0,T}, \tag{3.5}$$

Remark 3.1 This proposition offers a unified framework for obtaining a posteriori error estimates by reconstruction using various finite element methods. It is clear that the error indicators defined in this proposition depend on the numerical method employed, as the reconstructions used to establish these indicators are based on the solutions obtained by the finite element method. Consequently, the comparison presented in this section serves both as a comparison of different error estimators and as a comparison of the underlying numerical methods.

4. Remarks on the comparison of two types of error estimates

- Residual-type error estimators are easy to compute since there is no need to reconstruct. In contrast to the reconstruction-based a posteriori error estimates, no additional subproblem has to be solved when dealing with residual-based error estimates.
- The reconstruction estimates given in the proposition (3.1) **are obtained with 1 as a multiplicative constant** unlike the residual type estimate given by the theorem (2.1).
- Concerning the estimation of residual type error, the error on the pressure is measured only in L^2-norm, since p given by (1.2) is only in $L^2(\Omega)$.
- Both types of estimates are efficient, i.e. there is a **lower error bound** by the indicators
- The indicator $\eta_{P,T}$ defined in (3.3) looks somehow like $\eta_{D,T}$ given by (2.3), except that the latter only measures the standard of $\mathbf{u}_h$ is constant by elements so its gradient vanish, so he does not give a good sense as estimators.

5. Finite Element Approximations and Associated Reconstructions

5.1. Raviart-Thomas Finite Elements

We consider problem (1.3), which consists in finding an approximation $(\mathbf{u}_h, p_h)$ such that $\mathbf{u}_h \in H(\mathrm{div}, \Omega)$ and $\int_T (\mathrm{div}\mathbf{u}_h + f)\, v_h = 0$, meaning that no flux reconstruction is required. However, $p_h \notin H_0^1(\Omega)$, and moreover, $\mathbf{u}_h \neq -\mathbf{K}\nabla p_h$, since p_h is piecewise constant and thus has a zero gradient. In this context, reconstruction of the potential is necessary.
Following [22,28], we consider a post-processing step to construct $\tilde{p}_h$ in order to locally recover the relation between $\mathbf{u}_h$ and $-\mathbf{K}\nabla\tilde{p}_h$. Subsequently, we reconstruct an equilibrated potential s_h according to the definition given in (3.1).
Let $(p_h, \mathbf{u}_h) \in Q_h \times V_h$ solution of the problem (1.2), we define the post-processing $\tilde{p}_h$ by:

$$\begin{cases} -\mathbf{K}_T \nabla \tilde{p}_h|_T = \mathbf{u}_h|_T & \forall T \in \mathcal{T}_h \\ \dfrac{(\tilde{p}_h, 1)_T}{|T|} = p_h|_T & \forall T \in \mathcal{T}_h \end{cases} \tag{5.1}$$

Remark 5.1

It is worth mentioning that $\tilde{p}_h$ is locally defined on each element $T \in \mathcal{T}_h$, which ensures that its construction remains computationally inexpensive.

The function $\tilde{p}_h$, as previously constructed, is not continuous across inter-element boundaries. To obtain a continuous approximation, we apply the Oswald interpolation operator to $\tilde{p}_h$. The resulting function, denoted by $I_{os}(\tilde{p}_h)$, belongs to the space $P_1(\mathcal{T}_h) \cap H^1(\Omega)$ and is defined at each interior mesh node a by

$$I_{os}(\tilde{p}_h)(a) = \frac{1}{|\mathcal{T}_a|} \sum_{T \in \mathcal{T}_a} \tilde{p}_h|_T(a), \tag{5.2}$$

where $\mathcal{T}_a$ denotes the set of elements sharing the vertex a.
We impose that at boundary nodes, the value of $I_{os}(\tilde{p}_h)$ is set to zero, which implies that $I_{os}(\tilde{p}_h) \in H_0^1(\Omega)$. This membership allows us to define the conforming reconstructed function as

$$s_h := I_{os}(\tilde{p}_h). \tag{5.3}$$

In the case of the Raviart–Thomas approximation, two reconstructions of the potential are available, denoted by $\tilde{p}_h$ and s_h. An alternative way to estimate the error on the potential is to evaluate $\|p - \tilde{p}_h\|_1$ instead of $\|p - s_h\|_1$. It should be noted that, in the case of $\|p - \tilde{p}_h\|_1$, the norm considered is the broken H^1 norm. Moreover, in this approximation setting, there is no need to reconstruct the flux, hence we set $\sigma_{\mathbf{h}} := \mathbf{u}_h$. Consequently, a variant of Proposition 3.1 (cf. [28]) can be stated as follows:

Proposition 5.1
Let p given by (1.2) and $\tilde{p}_h$ given by (5.1) and s_h given by (5.3).
Then

$$|||p - \tilde{p}_h|||_1^2 \leq \sum_{T \in \mathcal{T}_h} (\eta_{NC,T}^2 + (\eta_{DF,T} + \eta_{R,T})^2) \tag{5.4}$$

Where the nonconformity estimator given by:

$$\eta_{NC,T} := |||\tilde{p}_h - s_h|||_{1,T} \tag{5.5}$$

and the diffusive flux estimator:

$$\eta_{DF,T} := |||\sigma_{\mathbf{h}} + K\nabla\tilde{p}_h|||_{\star,T} \tag{5.6}$$

5.2. Elements of Crouzeix-Raviart

Before presenting a reconstruction for the Crouzeix-Raviart elements, the approximation p_h can be given as cf [14]

$$(K\nabla p_h, \nabla v_h) = (f, v_h), \quad \forall v_h \in V_h^{CR}, \tag{5.7}$$

where

$$V_h^{CR} = \{v \in P_1(\mathcal{T}_h) \mid \langle [v], 1\rangle_e = 0, \quad \forall e \in \mathcal{E}_h\}. \tag{5.8}$$

The potential p_h, as defined, is not equilibrated, since it does not belong to $H_0^1(\Omega)$. Likewise, the flux $-\mathbf{K}\nabla p_h$ is not equilibrated either, since it does not satisfy the axioms of Definition 3.1. We must therefore specify both the potential and flux reconstructions s_h and $\sigma_\mathbf{h}$.

We can **reconstruct the potential**, using just the Oswald operator (5.2):

$$s_h = I_{os}(p_h) \tag{5.9}$$

The reconstruction of the flux can be given by cf. [20])

$$\sigma_\mathbf{h}|_T = -K\nabla u_h|_T + \kappa_f|_T \tag{5.10}$$

where κ_f is the piecewise affine vector function given on each element $T \in \mathcal{T}_h$ by

$$\frac{f_{|T}}{2}(x - x_T)$$

and x_T is the barycenter of T.

Assuming that $f \in P_0(\mathcal{T}_h)$ and K is a scalar in $P_0(\mathcal{T}_h)$, then the flux σ_h defined by (5.10) is equilibrated cf. [20].

5.3. Discontinuous Galerkin method

Before introducing the discontinuous Galerkin (DG) method, we first define some notation. Let $e \in \mathcal{E}_h$, consider nonnegative weights $\omega_{T^-,e}$ and $\omega_{T^+,e}$ such that

$$\omega_{T^-,e} + \omega_{T^+,e} = 1.$$

The corresponding weighted average is given by

$$\{v\}_\omega = \omega_{T^-,e}\, v^- + \omega_{T^+,e}\, v^+.$$

A common choice is to set equal weights, $\omega_{T^-,e} = \omega_{T^+,e} = \frac{1}{2}$. In problems involving strongly heterogeneous diffusion tensors, it is often preferable to use diffusion-dependent weights, defined as

$$\omega_{T^+,e} = \frac{\delta_{\mathbf{K},e^-}}{\delta_{\mathbf{K},e^+} + \delta_{\mathbf{K},e^-}}, \quad \omega_{T^-,e} = \frac{\delta_{\mathbf{K},e^+}}{\delta_{\mathbf{K},e^+} + \delta_{\mathbf{K},e^-}},$$

where

$$\delta_{\mathbf{K},e^\pm} = \mathbf{n}_e^T\, (\mathbf{K}|_{T^\pm})\, \mathbf{n}_e.$$

On boundary faces, the jump reduces to $[v] = v$, the average becomes $\{v\}_\omega = v$, and the weight is set to $\omega_{T,e} = 1$, where T is the single adjacent element. In this case, the normal diffusion term is

$$\delta_{\mathbf{K},e} = \mathbf{n}_e^T(\mathbf{K}|_T)\mathbf{n}_e,$$

with $\mathbf{n}_e$ being the outward unit normal to the domain Ω.
Let α be a positive parameter, and $\theta \in \{-1, 0, 1\}$. Set

$$V_h^{DG} = \{v \in L^2(\Omega), \forall T \in \mathcal{T}_h, v_{|T} \in P_1(T)\}$$

Note that this space has no continuity requirements. The discontinuous Galerkin (DG) method consists in seeking $p_h \in V_h^{DG}$

$$\sum_{T\in\mathcal{T}_h}(K\nabla p_h,\nabla v_h)_T-\sum_{e\in\mathcal{E}_h}(<\{K\nabla p_h\}_\omega\cdot n_e,[v_h]>_e+\theta<\{K\nabla v_h\}_\omega\cdot n_e,[p_h]_e>)$$
$$+\sum_{e\in\mathcal{E}_h}<\alpha h_e^{-1}\gamma_{\mathbf{K},e}[p_h],[v_h]>_e=(f,v_h),\qquad\forall v_h\in V_h^{DG}\tag{5.11}$$

Where the penalty parameter $\gamma_{\mathbf{K},e}$ is defined as

$$\gamma_{\mathbf{K},e}=\begin{cases}\dfrac{\delta_{\mathbf{K},e^+}\delta_{\mathbf{K},e^-}}{\delta_{\mathbf{K},e^+}+\delta_{\mathbf{K},e^-}}, & \text{if } e \text{ is an interior face,}\\ \delta_{\mathbf{K},e}, & \text{if } e \text{ is a boundary face.}\end{cases}$$

We can **reconstruct the potential**, using just the Oswald operator (5.2):

$$s_h=I_{os}(u_h)\tag{5.12}$$

The flux $K\nabla p_h$ obtained is not equilibrated, an equilibrated one cf. [20,16] can be given by:

$$<\sigma_h\cdot n_e,q_h>_e=<-\{K\nabla u_h\}_\omega\cdot n_e+\alpha\,\gamma_{\mathbf{K},e}\,h_e^{-1}[u_h],q_h>_e\quad\forall q_h\in P_0(e)\tag{5.13}$$

6. Numerical results

In this section, we present a series of three numerical experiments aimed at evaluating the performance of various numerical methods and the corresponding error estimators.

In the first test, we consider a sufficiently regular analytical solution. A uniform mesh refinement is performed in order to study the convergence behavior of various error indicators as well as the exact errors, for all numerical methods considered in this paper.
The second test is conducted in two stages. First, using Raviart-Thomas finite elements, we compare two types of a posteriori error estimators: residual-based and flux reconstruction-based estimators, incorporating mesh adaptation strategies. In the second stage, focusing solely on reconstruction-based error estimators, we assess the performance of these indicators by applying them to different numerical approximation schemes.
This last analysis also constitutes the main objective of the third numerical test, which is devoted to a comparative study of reconstruction-based indicators across various numerical methods.

Notations:

The exact errors are defined as follows:

$$E_{p,L^2}=\|p-p_h\|_{0,\Omega}\quad E^c_{r,L^2}=\|p-s_h\|_{0,\Omega}$$
$$E^c_{r,H^1}=\|\!|p-s_h|\!\|_{1,\Omega}\quad E^d_{r,H^1}=\|\!|p-\tilde{p}_h|\!\|_{1,\Omega}$$
$$E_{v,div}=\|u-u_h\|_{\star,\mathrm{div}}\quad E_{v,L^2}=\|u-u_h\|_\star$$

The residual-type a posteriori error indicators, summed over all elements $T\in\mathcal{T}_h$, are defined as follows:

$$\eta^{\mathrm{Res}}_{\mathrm{Div}}=\sum_{T\in\mathcal{T}_h}\|f-\mathrm{div}(\mathbf{u}_h)\|_{0,T},\qquad\eta^{\mathrm{Res}}_{D}=\sum_{T\in\mathcal{T}_h}h_T\|\mathbf{u}_h\|_{0,T},\qquad\eta^{\mathrm{Res}}_{S}=\sum_{T\in\mathcal{T}_h}h_e^{1/2}\left\|\left[K^{-1}\mathbf{u}_h\cdot\mathbf{t}_{e_i}\right]\right\|_{0,\partial T}.$$

The reconstruction-based a posteriori error indicators, summed over all elements $T\in\mathcal{T}_h$, are defined as follows:

$$\eta_P^{(k)} = \sum_{T\in\mathcal{T}_h} \|\sigma_h + \mathbf{K}\nabla s_h\|_{\star,T}, \qquad \eta_{DF}^{(k)} = \sum_{T\in\mathcal{T}_h} \|\sigma_h + K\nabla\tilde{p}_h\|_{\star,T},$$

$$\eta_R^{(k)} = \sum_{T\in\mathcal{T}_h} \frac{h_T}{\pi c_{K,T}^{1/2}} \|f - \mathrm{div}\sigma_h\|_{0,T}, \qquad \eta_{NC}^{(k)} = \sum_{T\in\mathcal{T}_h} \|\tilde{p}_h - s_h\|_{0,T}.$$

$$\eta_D^{(k)} = \sum_{T\in\mathcal{T}_h} \|f - \mathrm{div}\sigma_h\|_{0,T},$$

In light of Remark 3.1, the error indicators depend on the chosen approximation method. To avoid any ambiguity,We introduce the superscript k in the context of reconstruction-based estimators to specify the numerical method employed, with $k =$ RT, CR, or DG corresponding respectively to the Raviart-Thomas, Crouzeix-Raviart, and Discontinuous Galerkin finite element methods. Accordingly, we denote by $\eta_t^{(k)}$ the sum of the local reconstruction-based error indicators associated with method k. In the context of the Raviart-Thomas finite element approximation, note that there is no need to reconstruct the flux, so that $\sigma_{\mathbf{h}} = \mathbf{u}_h$. For the other proposed approximations, it can be readily shown that only the indicators $\eta_P^{(k)}$, $\eta_R^{(k)}$, and $\eta_D^{(k)}$ provide an upper bound for the error, where $k =$ CR or DG.

We further introduce the following notations: N_T denotes the total number of mesh elements, and h is the mesh size. The quantity η_t refers to the total error indicator, defined as the sum of all local indicators over the mesh. The efficiency index I is defined as the ratio between the upper bound provided by the a posteriori error estimates-specifically those established in Propositions 2.1 and 3.1 and the sum of the corresponding exact errors.

6.1. Numerical experiments 1

In order to test the exact convergence of errors, we consider the problem (1.1) with $K = Id$ with a manufactured solution,

$$p_{ex} = x(x-1)y(y-1) \quad in\ \Omega =]0,1[^2 \tag{6.1}$$

whence the exact flux is given by

$$u_{ex} = \begin{pmatrix} (2x-1)y(y-1) \\ (2y-1)x(x-1) \end{pmatrix}. \tag{6.2}$$

and the second member $f = -2y(y-1) - 2x(x-1)$

6.1.1. Raviart Thomas finite elements.
Figure 1a shows the initial mesh. The exact potential is depicted in Figure 1c and defined by equation (6.1), while the exact flux is shown in Figure 1b. Subsequently, Figure 1c allows for a comparison between the exact potential, the potential obtained using the Raviart–Thomas finite element method (Figure 1d), the post-processed solution (Figure 1e), and the reconstructed solution given in (Figure 1f).
Tables 1 and 2 report the results of a uniform mesh refinement using Raviart-Thomas finite elements as defined by equations (1.3). The first table corresponds to the results related to the a posteriori error estimates based on reconstructions, while the second one presents the results associated with the classical residual-based estimators.
As shown in Table 1, we numerically observe that $E_{r,H^1}^d = E_{v,L^2}$. This result can be rigorously justified by noting that $-\mathbf{K}\nabla p = \mathbf{u}$ and $-\mathbf{K}\nabla\tilde{p}_h = \mathbf{u}_h$, together with the definitions of the norms $||\cdot||_1$ and $|||\cdot|||_\star$ provided in (1.4) and (1.5).

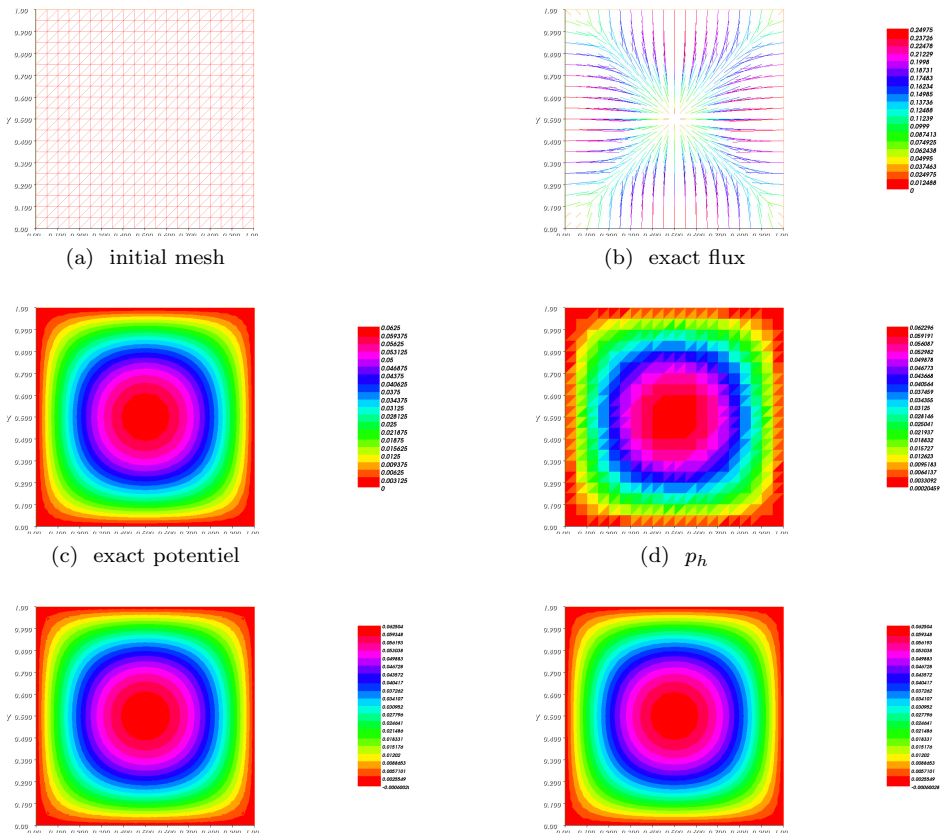

(a) initial mesh (b) exact flux

(c) exact potentiel (d) p_h

(e) $\tilde{p}_h$ post processing (f) s_h reconstruction of potentiel

Figure 1: Mesh, exact solution, and corresponding approximations

Table 1: Uniform refinement RT_0

E_{p,L^2}	E^c_{r,L^2}	E^c_{r,H^1}	E^d_{r,H^1}	E_{v,L^2}	$E_{v,div}$	N_T	h
0.00349943	0.000551791	0.0235952	0.0147757	0.0147757	0.0147757	200	0.141421
0.00175508	0.000136242	0.0120659	0.00743696	0.00743696	0.00743696	800	0.0707107
0.0011707	6.02751e-005	0.00808181	0.00496411	0.00496411	0.00496411	1800	0.0471405
0.000878192	3.40794e-005	0.00607177	0.0037247	0.0037247	0.0037247	3200	0.0353553
0.000702616	2.18481e-005	0.00486138	0.00298036	0.00298036	0.00298036	5000	0.0282843

$\eta_P^{(RT)}$	$\eta_{DF}^{(RT)}$	$\eta_R^{(RT)}$	$\eta_{NC}^{(RT)}$	$\eta_D^{(RT)}$	$\eta_t^{(RT)}$	**I**
0.0271402	1.82979e-016	0.00172658	0.0271402	0.0383551	0.0542888	0.998703
0.0140835	4.60221e-016	0.000432786	0.0140835	0.0192282	0.0276875	0.978976
0.00945766	7.24975e-016	0.000192443	0.00945766	0.012825	0.0185314	0.975284
0.00711178	9.79837e-016	0.000108268	0.00711178	0.0096204	0.0139183	0.973983
0.00569639	1.31225e-015	6.92967e-005	0.00569639	0.00769693	0.011142	0.973378

Table 2: Refinement uniform residu type estimation

E_{p,L^2}	$E_{v,div}$	$E_{p,L^2} + E_{v,div}$	$\eta_{\text{Div}}^{\text{Res}}$
0.00349943	0.0147757	0.0182752	0.0383551
0.00175508	0.00743696	0.00919204	0.0192282
0.0011707	0.00496411	0.00613481	0.012825
0.000878192	0.0037247	0.00460289	0.0096204
0.000702616	0.00298036	0.00368298	0.00769693

η_S^{Res}	η_D^{Res}	$\widehat{\eta^{Res}}$	N_T,	h	I
0.0648169	0.0210692	0.0782065	200	0.141421	4.27939
0.0353874	0.0105394	0.0416301	800	0.0707107	4.52893
0.0242029	0.00702685	0.0282778	1800	0.0471405	4.60941
0.0183735	0.00527028	0.0213989	3200	0.0353553	4.64901
0.0148028	0.00421628	0.0172088	5000	0.0282843	4.67251

6.1.2. Crouzeix-Raviart finite elements.
Figures 2a, 2b, 2c, and 2d respectively illustrate: the potential approximated using Crouzeix-Raviart finite elements as defined in (5.7); the reconstructed potential given by (5.9); the exact flux defined in (6.2); and the reconstructed flux according to (5.10).
Table 3 presents the numerical results obtained from a uniform mesh refinement applied to the reconstruction-based error estimators using Crouzeix-Raviart finite elements.

6.1.3. Discontinuous Galerkin finite elements.
Figures 3a, 3b, 3c, and 3d respectively display: the potential approximated by the discontinuous Galerkin (DG) finite element method as defined in (5.11); the reconstructed potential described in (5.12); the exact flux defined in (6.2); and the reconstructed flux obtained via the formula outlined in (5.13).
Table 4 reports the numerical results derived from a uniform mesh refinement applied to the reconstruction-based a posteriori error estimators using the DG finite element method.

6.1.4. Remarks on the Results of the First Numerical Test.
The following conclusions can be drawn from Tables 1, 2, 3, and 4 related to the first numerical test:

- All exact errors converge with an order close to 1, except for E^c_{r,L^2}, which exhibits second-order convergence. This is consistent with the theoretical results (see [28]).
- The quantity $\bar{\eta}_{DF}$ in Table 1 is practically zero, which can be explained by the first equation in 5.1.
- The sum of the local error indicators η_t in each case converges with a rate close to 1. This confirms that the indicators are reliable approximations of the actual error, in agreement with a priori error

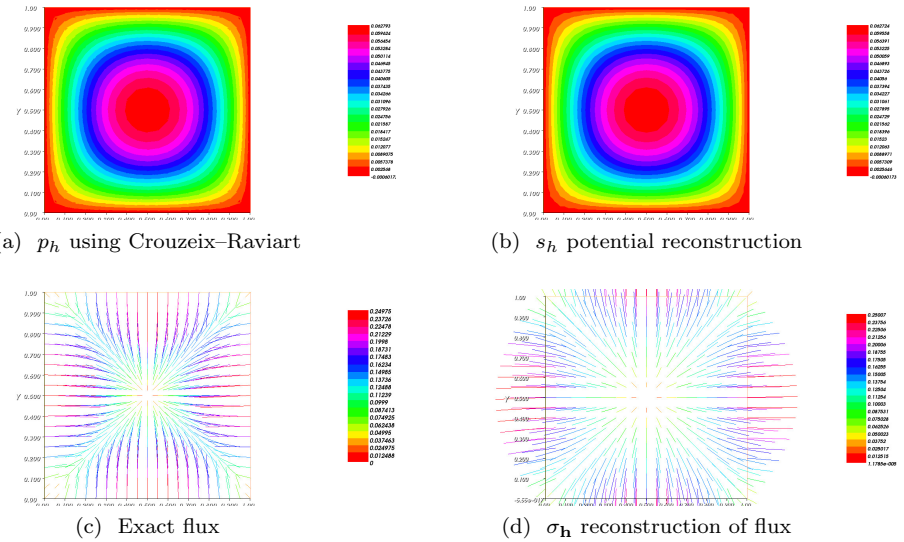

(a) p_h using Crouzeix–Raviart (b) s_h potential reconstruction

(c) Exact flux (d) $\sigma_{\mathbf{h}}$ reconstruction of flux

Figure 2: Meshes

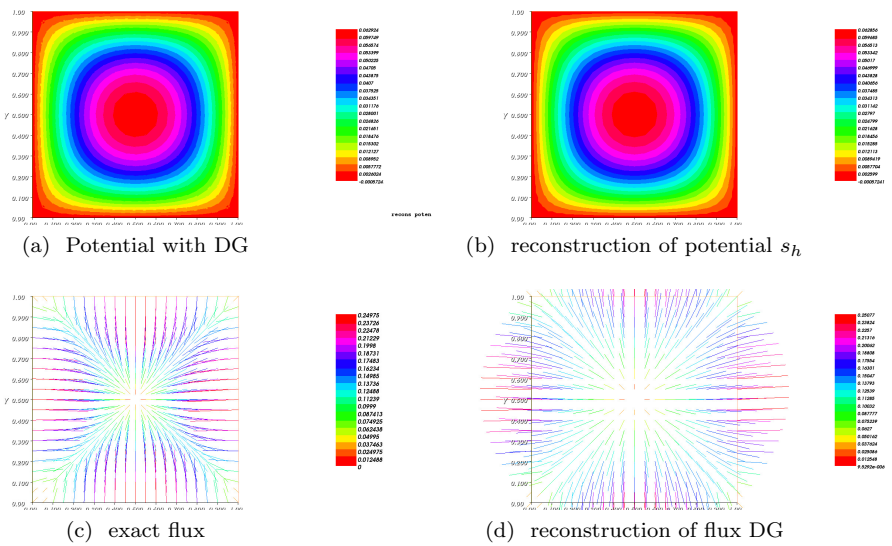

(a) Potential with DG (b) reconstruction of potential s_h

(c) exact flux (d) reconstruction of flux DG

Figure 3: xact solution and approximations for DG

Table 3: Refinement uniform - Crouzeix Raviart

E_{p,L^2}	E^c_{r,H^1}	$E_{v,div}$	$E^c_{r,H^1} + E_{v,div}$
0.00039412	0.000347519	0.0259866	0.0263807
9.93916e-005	8.2599e-005	0.0139601	0.0140595
4.42468e-005	3.62609e-005	0.00951917	0.00956341
2.49032e-005	2.03009e-005	0.00721854	0.00724344
1.59423e-005	1.2963e-005	0.00581269	0.00582863

$\eta_P^{(CR)}$	$\eta_R^{(CR)}$	$\eta_D^{(CR)}$	$\eta_t^{(CR)}$	h	I
0.03377	0.00384828	0.0384194	0.0512959	0.141421	1.03454
0.0182562	0.00120161	0.0192362	0.0265474	0.0707107	1.02002
0.0124227	0.000612629	0.0128274	0.0178673	0.0471405	1.01513
0.0094029	0.000382385	0.0096214	0.0134585	0.0353553	1.01265
0.00756118	0.000266395	0.00769744	0.0107932	0.0282843	1.01116

Table 4: Refinement uniform-DG method

E_{p,L^2}	E^c_{r,H^1}	$E_{v,div}$	$E^c_{r,H^1} + E_{v,div}$
0.000787911	0.000743522	0.0150062	0.0157941
0.0001991	0.000180226	0.00749932	0.00769842
8.89473e-005	7.89152e-005	0.00499329	0.00508224
5.02875e-005	4.40016e-005	0.00374166	0.00379194
3.23476e-005	2.79957e-005	0.00299146	0.00302381

$\eta_P^{(DG)}$	$\eta_R^{(DG)}$	$\eta_D^{(DG)}$	$\eta_t^{(DG)}$	h	I
0.0271594	0.00218056	0.0384194	0.0471003	0.141421	1.2222
0.0141243	0.000624732	0.0192362	0.0238729	0.0707107	1.22107
0.00948431	0.000315605	0.0128274	0.015956	0.0471405	1.22058
0.0071302	0.000198693	0.0096214	0.0119771	0.0353553	1.2204
0.00570997	0.000140249	0.00769744	0.00958509	0.0282843	1.22033

estimates which predict a convergence order of 1 for the exact error.

- For the tables corresponding to estimators based on reconstruction (Tables 1, 3, and 4), the effectivity index I is close to 1. This is not the case in Table 2, which presents classical residual-based estimators. The difference can be attributed to the fact that reconstruction-based estimators are derived with a multiplicative constant equal to 1, unlike classical residual-based estimators, where this constant is not controlled. This represents a fundamental distinction between the two approaches.

6.2. Numerical experiments 2

In order to assess the performance of the two types of estimators under mesh adaptation, we consider an exact solution given by:

$$p_{ex} = \exp\left(-\frac{1-x}{\sqrt{\varepsilon}}\right) + \exp\left(-\frac{1-y}{\sqrt{\varepsilon}}\right), \quad \varepsilon = 10^{-3}.$$

In this numerical test, non-homogeneous Dirichlet boundary conditions are imposed. Accordingly, we introduce a data oscillation indicator defined as:

$$\eta_{os} = \|g - P^0_{h,\partial\Omega} g\|_{0,T\cap\partial\Omega},$$

where $P^0_{h,\partial\Omega} g$ denotes the piecewise constant L^2-projection of g on the boundary mesh.

For the two numerical tests presented in the following sections, we employ an adaptive mesh refinement procedure based on local error indicators. The goal is to iteratively improve the accuracy of the numerical solution by refining the mesh where the estimated error is significant. The adaptive process is governed

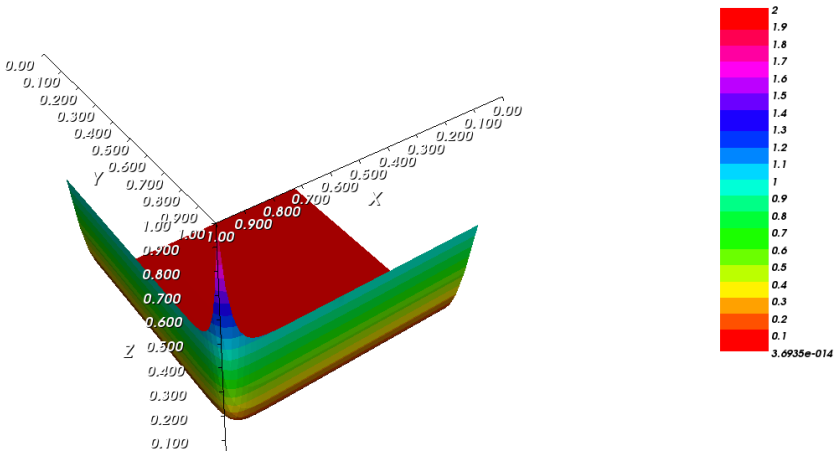

(a) Exact potentiel

by the algorithm `RemeshIndicator`, described below.

...

Algorithm: RemeshIndicator

1. Choose the maximum number of iterations $k_{\max}$ and a tolerance threshold tol.
2. Generate an initial mesh $\mathcal{T}_h^0$.
3. Set the iteration counter $k = 0$.
4. Solve the discretized problem on the current mesh $\mathcal{T}_h^k$.
5. For each element $T \in \mathcal{T}_h^k$, compute the local error indicator $\eta_T^{(k)}$.
6. If $\sum_{T\in\mathcal{T}_h^k} \eta_T^{(k)} \leq tol$ or if $k = k_{\max}$, then stop the algorithm.
7. Otherwise, increment the iteration counter: $k \leftarrow k + 1$.
8. Determine the new local mesh sizes $h_T^{(k)}$ from the local error indicators using the formula:

$$h_T^{(k)} = \frac{1}{f_{ind}}, \quad \text{where} \quad f_{ind} = \max\left(\min\left(\frac{\eta_T}{\eta^\star}, 3\right), \frac{1}{3}\right),$$

   and $\eta^\star = cc \cdot \frac{1}{|\mathcal{T}_h^k|} \sum_{T\in\mathcal{T}_h^k} \eta_T^{(k)}$ with $0 < cc \leq 1$.
9. Generate a new mesh $\mathcal{T}_h^k$ based on the updated element sizes.
10. Return to step 4.

Figures 4a, 4b, 4c, and 4d display the sum of the residual-based and reconstruction-based error indicators, computed using the Raviart-Thomas, Discontinuous Galerkin, and Crouzeix-Raviart approximations, respectively. It is clearly observed that all these indicators capture the boundary layer.

To further assess the effectiveness of these indicators, we perform mesh adaptation using the RemeshIndicator algorithm, and compute the exact error at each refinement step. Figure 5a illustrates, for the same RT_0 approximation, a comparison between the two types of indicators. The exact error $E^c_{r,H^1} + E_{v,div}$ is plotted against the number of elements on a logarithmic scale. Note that, in the case of the residual-type estimator, the term E^c_{r,H^1} corresponds to the H^1-norm error given by $\|p - p_h\|_1 = \sum_{T\in\mathcal{T}_h} \|p - p_h\|_{1,T}$. This figure shows that mesh adaptation driven by reconstruction-based indicators leads to a significantly lower error compared to that obtained using classical residual-type indicators. This observation can be explained by the fact that the error is evaluated in the H^1 norm on the potential, while p_h is a piecewise constant function, implying that its gradient is zero. Moreover, the estimate provided by Proposition 2.1 is only valid in the L^2 norm. To clarify this point, we have plotted in Figure 5b the two errors in the L^2

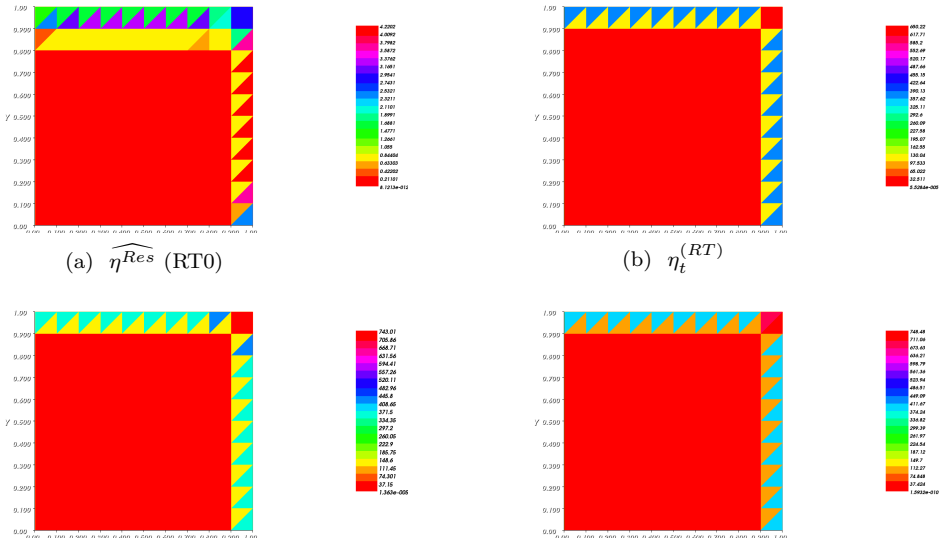

(a) $\widehat{\eta^{Res}}$ (RT0) (b) $\eta_t^{(RT)}$

(c) $\eta_t^{(DG)}$ Sum of Indicators (DG) (d) $\eta_t^{(CR)}$ Sum of Indicators (Crouzeix-Raviart)

Figure 4: The total indicator values in each case

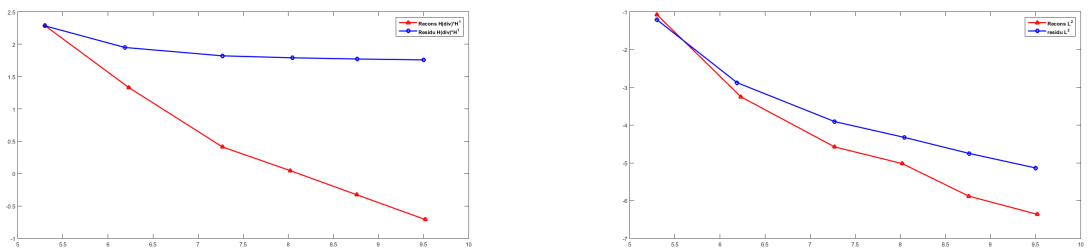

(a) $E^c_{r,H^1} + E_{v,div}$ using both types of estimators (b) $\|p - s_h\|_0$ and $\|p - p_h\|_0$

Figure 5: Comparison: reconstruction-based and residual-based estimators

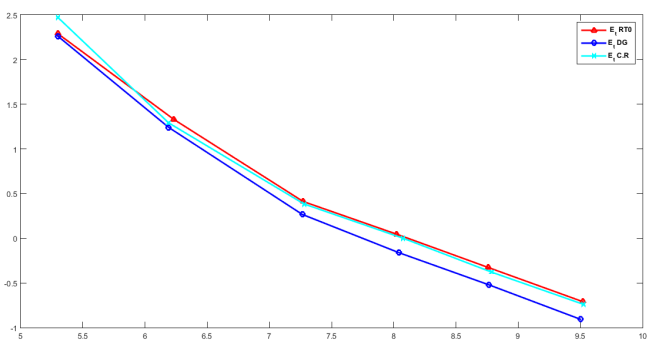

Figure 6: Comparison Among Different Reconstruction Estimators

norm. This figure clearly shows that the reconstruction-based estimators are consistently more effective, even when the errors are assessed solely in the L^2 norm.
The final figure of this numerical experiment, namely Figure 6, presents a comparison of the efficiency of reconstruction-based estimators under mesh adaptation. The RemeshIndicator algorithm is consistently applied for each numerical approximation method considered: Raviart-Thomas, Crouzeix-Raviart, and discontinuous Galerkin. It can be observed that the estimator based on the discontinuous Galerkin method is slightly more efficient than the other two. This comparison of reconstruction-based estimators is also the focus of the final numerical test.

6.3. Numerical experiments 3

We consider the problem (1.1) with $K = 100 \times \chi_{(x>0.5)} + 1 \times \chi_{(x<0.5)}$ with a manufactured solution, $p_{ex} = \sin(\pi x)\sin(\pi y)$ in $\Omega =]0,1[^2$ whence the exact flux is given by $u_{ex} = K\nabla p_{ex}$ and the second member $f = (K\pi^2 + K\pi^2)p_{ex}$
Figures 7a, 7b, and 7c depict the coefficient K, the exact potential, and the exact flux, respectively. A

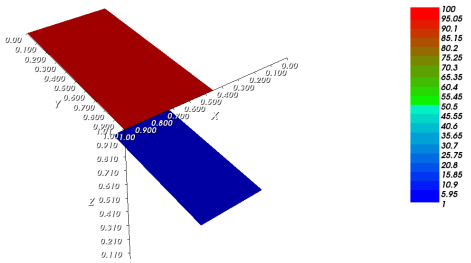

(a) K

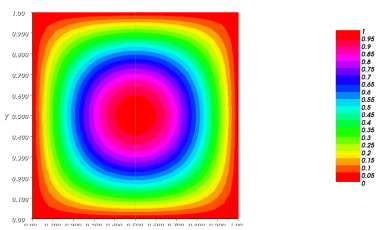

(b) Exact potentiel (p_{ex})

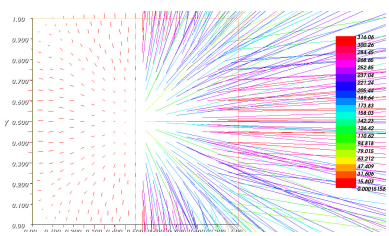

(c) Exact flux u_{ex}

Figure 7: Exact solution

strong discontinuity in the flux is observed at the center, which originates from the expression of K.

Figure 8 displays the exact errors obtained with various reconstruction-based estimators. Once again, the estimator employing the discontinuous Galerkin method demonstrates superior efficiency compared to the other approaches.

7. Conclusion

In this work, we presented two types of error estimators: residual-based and reconstruction-based estimators. A theoretical comparison of the results was also provided. Numerical tests demonstrated the superior efficiency of the reconstruction-based estimators. Furthermore, by considering various finite element methods, Raviart-Thomas, Crouzeix-Raviart, and discontinuous Galerkin, we compared the performance of the reconstruction-based estimators associated with each method. It was concluded that the most effective approach is to employ reconstruction-based estimators with the discontinuous Galerkin approximation.

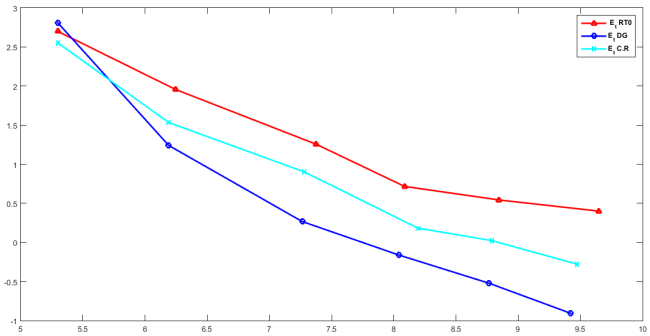

Figure 8: Comparison among different reconstruction estimators

References

1. Achchab, B., Achchab, S., and Agouzal, A., *Some remarks about the hierarchical a posteriori error estimate*, Numerical Methods for Partial Differential Equations **20** (2004), no. 6, 919–932.
2. Alonso, A., *Error estimators for a mixed method*, Numerische Mathematik **74** (1996), 385–395.
3. Araya, R., Poza, A. H., and Stephan, E. P., *A hierarchical a posteriori error estimate for an advection-diffusion-reaction problem*, Mathematical Models and Methods in Applied Sciences **15** (2005), no. 7, 1119–1139.
4. Babuška, I., and Rheinboldt, W. C., *Error estimates for adaptive finite element computations*, SIAM Journal on Numerical Analysis **15** (1978), no. 4, 736–754.
5. Bank, R. E., and Weiser, A., *Some a posteriori error estimators for elliptic partial differential equations*, Mathematics of Computation **44** (1985), no. 170, 283–301.
6. Boffi, F., and Bertrandand, D., *The Prager-Synge theorem in reconstruction based a posteriori error estimation*, in: 75 Years of Mathematics of Computation: Symposium on Celebrating 75 Years of Mathematics of Computation, November 1–3, 2018, Institute for Computational and Experimental Research in Mathematics (ICERM), vol. 754, American Mathematical Society, 2020.
7. Bergam, A., Bernardi, C., and Mghazli, Z., *A posteriori analysis of the finite element discretization of some parabolic equations*, Mathematics of Computation **74** (2005), no. 251, 1117–1138.
8. Brandts, J. H., *Superconvergence and a posteriori error estimation for triangular mixed finite elements*, Numerische Mathematik **68** (1994), no. 3, 311–324.
9. Braess, D., and Schöberl, J., *Equilibrated residual error estimators for Maxwell's equations*, Technical Report 2006-19, Johann Radon Institute for Computational and Applied Mathematics (RICAM), 2006.
10. Braess, D., and Verfürth, R., *A posteriori error estimators for the Raviart-Thomas element*, SIAM Journal on Numerical Analysis **33** (1996), no. 6, 2431–2444.
11. Brezzi, F., and Fortin, M., *Mixed and hybrid finite element methods*, Springer-Verlag, New York, 1991.
12. Carstensen, C., *All first-order averaging techniques for a posteriori finite element error control on unstructured grids are efficient and reliable*, Mathematics of Computation **73** (2004), no. 247, 1153–1165.
13. Carstensen, C., *A posteriori error estimate for the mixed finite element method*, Mathematics of Computation **66** (1997), no. 218, 465–476.
14. Crouzeix, M., and Raviart, P. A., *Conforming and nonconforming finite element methods for solving the stationary Stokes equations*, RAIRO Modél. Math. Anal. Numér. **3** (1973), 33–75.
15. Destuynder, P., and Métivet, B., *Explicit error bounds in a conforming finite element method*, Mathematics of Computation **68** (1999), no. 228, 1379–1396.
16. Ern, A., Nicaise, S., and Vohralík, M., *An accurate* **H**(div) *flux reconstruction for discontinuous Galerkin approximations of elliptic problems*, Comptes Rendus Mathématique **345** (2007), no. 12, 709–712.
17. Hecht, F., Mghazli, Z., Naji, I., and Roberts, J. E., *A residual a posteriori error estimators for a model for flow in porous media with fractures*, Journal of Scientific Computing **79** (2019), 935–968.
18. Hoppe, R. H., and Wohlmuth, B., *Element-oriented and edge-oriented local error estimators for nonconforming finite element methods*, ESAIM: Mathematical Modelling and Numerical Analysis **30** (1996), no. 2, 237–263.
19. Huang, W., Kamenski, L., and Lang, J., *A new anisotropic mesh adaptation method based upon hierarchical a posteriori error estimates*, Journal of Computational Physics **229** (2010), no. 6, 2179–2198.

20. Kim, K., *A posteriori error analysis for locally conservative mixed methods*, Mathematics of Computation **76** (2007), no. 257, 43–66.

21. Kirby, R., *Residual a posteriori error estimates for the mixed finite element method*, Computational Geosciences **7** (2003), 197–214.

22. Lovadina, C., and Stenberg, R., *Energy norm a posteriori error estimates for mixed finite element methods*, Mathematics of Computation **75** (2006), no. 256, 1659–1674.

23. Luce, R., and Wohlmuth, B. I., *A local a posteriori error estimator based on equilibrated fluxes*, SIAM Journal on Numerical Analysis **42** (2004), no. 4, 1394–1414.

24. Mghazli, Z., and Naji, I., *Analyse a posteriori d'erreur par reconstruction pour un modèle d'écoulement dans un milieu poreux fracturé*, Comptes Rendus Mathématique **355** (2017), no. 3, 304–309.

25. Mghazli, Z., and Naji, I., *Guaranteed a posteriori error estimates pour a fractured porous medium*, Mathematics and Computers in Simulation **164** (2019), 163–179.

26. Verfürth, R., *A posteriori error estimation and adaptive mesh-refinement techniques*, Journal of Computational and Applied Mathematics **50** (1994), no. 1–3, 67–83.

27. Verfürth, R., *A posteriori error estimators for convection-diffusion equations*, Numerische Mathematik **80** (1998), 641–663.

28. Vohralík, M., *Unified primal formulation-based a priori and a posteriori error analysis of mixed finite element methods*, Mathematics of Computation **79** (2010), no. 272, 2001–2032.

29. Wohlmuth, B. I., *Hierarchical a posteriori error estimators for mortar finite element methods with Lagrange multipliers*, SIAM Journal on Numerical Analysis **36** (1999), no. 5, 1636–1658.

30. Wohlmuth, B., and Hoppe, R., *A comparison of a posteriori error estimators for mixed finite element discretizations by Raviart-Thomas elements*, Mathematics of Computation **68** (1999), no. 228, 1347–1378.

Ilyas NAJI,
Laboratory of Education, Sciences and Techniques (LEST),
Higher School of Education and Training of Berrechid (ESEFB),
Hassan First University, Avenue de l'Université, 218 Berrechid,
26100, Morocco.
https://orcid.org/0000-0002-1020-263X
E-mail address: i.naji.univ@gmail.com